Structure-performance relationships on Co based Fischer – Tropsch synthesis catalysts: The more defect free the better

Tsakoumis, Nikolaos E.; Patanou, Eleni; Lögdberg, Sara; Johnsen, Rune E.; Myrstad, Rune; van Beek, Wouter; Rytter, Erling; Blekkan, Edd A.

Published in:
ACS Catalysis

Link to article, DOI:
10.1021/acscatal.8b03549

Publication date:
2019

Document Version
Peer reviewed version

Article

Structure-performance relationships on Co based Fischer – Tropsch synthesis catalysts: The more defect free the better

Nikolaos E. Tsakoumis, Eleni Patanou, Sara Lögdberg, Rune E. Johnsen, Rune Myrstad, Wouter van Beek, Erling Rytter, and Edd Anders Blekkan

ACS Catal., **Just Accepted Manuscript** • DOI: 10.1021/acscatal.8b03549 • Publication Date (Web): 03 Dec 2018

Structure-performance relationships on Co based Fischer – Tropsch synthesis catalysts: The more defect free the better

Nikolaos E. Tsakoumis[a,*], Eleni Patanou[a], Sara Lögdberg[b], Rune E. Johnsen[c], Rune Myrstad[d], Wouter van Beek[e], Erling Rytter[a,d], Edd A. Blekkan[a]

[a]*Department of Chemical Engineering, Norwegian University of Science and Technology (NTNU), NO-7491 Trondheim, Norway.*
[b]*Chemical Technology, KTH (Royal Institute of Technology), Teknikringen 42, SE-100 44 Stockholm, Sweden.*
[c]*Department of Energy Conversion and Storage, Technical University of Denmark, DK-4000 Roskilde, Denmark.*
[d]*SINTEF Materials and Chemistry, NO-7465 Trondheim, Norway.*
[e]*The Swiss-Norwegian Beamlines (SNBL) at ESRF, Grenoble F38043, France*

ABSTRACT Understanding and utilizing structure-performance relationships in catalytic nanomaterials is the epitome of catalysis science. Knowledge at the atomic level can potentially allow rational design of more selective and energy efficient catalytic materials. Fischer – Tropsch synthesis on cobalt is an example of a complicated system that operates in a narrow process regime, and the nature of the reaction product is governed by numerous parameters. On an industrial model catalyst, we have simplified the structure of the active, metallic nanoparticles into predominantly hexagonal close packed structure via the use of a Co_2C precursor. By varying the final reduction temperature, we could mildly modify catalyst microstructural properties at the nanoparticle (NP) level. Catalytic materials, although with minimal structural differences, showed significantly different performance. Evidently there is a narrow window for complete utilization of the hexagonal close packed Co crystallites that lays between removal of lattice carbon, that remains from the Co_2C precursor, and the initiation of stacking disorder, due to transition to the face centered cubic Co structure. Fischer – Tropsch synthesis performance indicators show that Co NPs with minimum number of crystal defects outperform catalysts with lattice defects, either due to the existence of lattice carbon or stacking faults. Therefore, catalyst preparation and activation procedures probably should be designed targeting defect free Co crystallites.

KEYWORDS: *Fischer–Tropsch synthesis, Cobalt, hcp, fcc, structure-performance relationships, stacking faults, lattice carbon, H_2 coverage.*

1. Introduction

Chemical reactions catalyzed by supported metal nanoparticles (NPs) exhibit variations in reaction kinetics that depend on the exposed surface structures. This structure sensitivity comes in different degrees, from minor/negligible (structure insensitive) to orders of magnitude (structure sensitive)[1,2]**.** For the structure sensitive reactions catalyst performance strongly depends on NP size, since the relative ratio of terraces, steps and kinks changes with NP size[3]. Similarly, crystallographic structure and particle shape have an analogous impact. Molecular level understanding at the nanoscale is needed for the establishment of structure performance relationships[4] that may lead to rational catalyst design. Such understanding has been previously obtained by theoretical[5,6] and/or experimental methods[7–10].

Fischer - Tropsch synthesis (FTS) is a process that converts synthesis gas (mixtures of CO and H_2) into linear hydrocarbons[11,12]. FTS follows a polymerization mechanism where a C_1 unit is added to a growing chain. As such, the products follow the Anderson–Schultz–Flory (ASF) distribution and the polymerization probability α can be derived if one knows hydrocarbon selectivities. The process has found application in conversion of natural gas into value added fuels and chemicals. In recent years, FTS is seen as an attractive option for production of ultraclean hydrocarbon mixtures from non-fossil feedstocks such as biomass and CO_2 and H_2O[13]. However, the complexity of the reaction is rendering FTS as one of the most challenging heterogeneous catalyzed systems.

In FTS, structure-performance relationships have been in the focus of research for many decades[14–17]. Several structural parameters appear to affect intrinsic performance and these include Co NP size, Co crystal phase, Co-support interaction and porous network/support variables. The size effect on Co NPs rich in face-centered cubic configuration has been extensively studied[10,18–21] . It was shown that the size of Co NPs is influencing performance in all aspects; activity[10], selectivity[22] and stability[23]. Co crystallizes in three different phases; face-centered cubic (*fcc*), hexagonal closed packed (*hcp*), and epsilon[24]. FTS sensitivity over the last two phases is less studied since at the nanoscale (< 20 nm) Co NPs stabilize into an

intergrown structure with *fcc*-Co as the major phase. Production of *hcp* rich Co NPs can be achieved from decomposition of Co carbide precursors (produced by carburization of the metallic NPs) under H_2. This alternative multistep activation was first studied by Hofer and Peebles[14] and reinvestigated, leading to uncover of phase sensitivity in FTS by Ducreux *et al.*[25]. The differences in rate and selectivity between NPs of *fcc*-Co and *hcp*-Co structures, although challenging to interpret, appear clear[26–29].

Support effects are more difficult to study since many parameters are affected from one support to the other in terms of acidity, metal-support interactions, porous network and Co particle size[30–32]. For Al_2O_3 based supports[33], the *fcc* rich Co NPs deriving from the commonly applied H_2 reduction of Co_3O_4 precursor are hybrid *fcc-hcp* structures with high concentration of stacking faults that are support dependent[25,34,35]. As mentioned above, predominately *hcp*-Co NPs can be prepared when a reduction – carburization – reduction (RCR) activation protocol is followed. However, to achieve the best catalytic properties, carbon produced during the carburization (CO disproportionation) step has to be minimized [29].

Regardless of differences in FTS performance, *hcp*-Co NPs produced by RCR appear as a better model system (in terms of crystallite purity) since they lack the intensely intergrown complex structures seen after H_2 reduction of Co_3O_4. This allows the construction of model systems with controlled differences solely at NP level.

In the present study, an industrial model Re/Co/γ-Al_2O_3 FTS catalyst was prepared by aqueous incipient wetness co-impregnation of cobalt and rhenium salts on γ-Al_2O_3 to give 20 wt.% Co and 0.5 wt.% Re. The catalyst was dried (100°C) and calcined (300°C), resulting in a precursor containing Co_3O_4 NPs. H_2 reduction at 350°C followed before carburization under CO at 14 bar and 230°C[29]. The prepared γ-Al_2O_3 supported Co_2C NPs were decomposed under H_2 at different temperatures forming *hcp* rich metallic Co NPs. Their kinetic performance in FTS and microstructural properties of the active catalytic materials were evaluated by fixed-bed reactor tests and synchrotron X-ray based characterization, respectively. A reference analogue (REF), where the Co_3O_4 precursor was reduced under H_2 and tested in FTS without any other treatment, was used for benchmarking[29]. By tuning preparation conditions, specifically the final reduction temperature, the catalysts gain their main properties, only differing in the microstructure of the Co NPs.

2. Experimental Section

Catalyst synthesis

The γ-alumina supported catalyst was prepared by incipient wetness (IW) co-impregnation of cobalt and rhenium salts. In detail, a γ-Al_2O_3 (Puralox SCCa, S_{BET} = 170 m^2/g, pore volume of 0.73 cm^3/g and 12 nm average pore size) support was impregnated with an aqueous solution of $Co(NO_3)\cdot 6H_2O$ and $HReO_4$ to give a loading of 20 wt. % Co and 0.5 wt. % Re. Subsequently, the catalyst was dried in an oven at 120 °C for 4 h and calcined in flowing air at 300 °C for 16 h with a ramping rate of 120 °C/h. For operation in diffusion limitation free regime, the catalyst samples were sieved to a particle diameter of 53−90 µm. More details on catalyst synthesis can be found in a different source [29].

Catalyst characterization

Hydrogen chemisorption was performed using a Micromeritics 2020 unit at 40 °C. Prior to the analysis, the reference and carburized samples were reduced under H_2 flow at 350 °C for 10 h. The cobalt dispersion was calculated by assuming dissociative adsorption of H_2 on the cobalt metal surface [36] and that rhenium does not contribute to the amount of hydrogen adsorbed. Re acts as a promoter increasing the exposed surface area of Co [37]. The average cobalt metal particle size (d(Co^o) nm) was calculated from the Co metal dispersion (D%) by assuming spherical, uniform Co metal nanoparticles with a site density of 14.6 atoms/nm^2 [36].

Synchrotron X-ray based characterization was performed at the Swiss-Norwegian Beamlines (SNBL) located at the European Synchrotron Radiation Facility (ESRF) in Grenoble, France. Station BM01B was used for the combined XANES and XRD. For the measurements, a quartz capillary (0.7 mm o.d.) based *in situ* cell was used. A detailed description of the set up can be found elsewhere [34,38].

In situ X-ray diffraction - Temperature programmed reduction (XRD-TPR). The carburized catalyst was inserted in the quartz capillary and temperature was increased from 30 °C to 700 °C at a heating rate of 3 °C /min under a flow of 2.5 ml/min pure hydrogen at ambient pressure. X-ray diffractograms were recorded throughout the TPR run. For *in situ* reduction experiment, similarly to XRD-TPR, the same setup and TPR profile configuration was used but different set-point temperatures i.e. 200 °C, 250 °C, 350 °C and 450 °C. The temperature was held at set point for 1 h (R250, R350 and R450) or 1.5 h (R200) before returning to 50

°C for the final measurement of X-ray diffractogram and X-ray absorption spectra.

X-ray absorption spectra were recorded at the Co K-edge (E = 7709 eV) using a double crystal Si (111) monochromator. The data collection was carried out in the transmission mode. Ion chamber detectors with their gases at ambient temperature and pressure were used for measuring the intensities of the incident (I_0) and transmitted (I_t) X-rays. Spectra from a cobalt foil (*hcp*) was used as $Co^{(0)}$ reference. The energy calibration was done by measuring the spectrum of the cobalt foil with the energy of the peak of the first derivative as the edge energy (7709 eV). The Demeter software (0.9.24) from the Ifeffit software package (Version 1.2.11) [39], was used for the XAS data analysis.

X-ray diffractograms were obtained using two independent Si (111) monochromators. XRD data were collected using a wavelength of 0.505 Å. A Si (111) standard was used for beam calibration. 2D images were obtained from a Dexela 2923 two-dimensional CMOS X-ray detector and converted to normal diffraction patterns using the program FIT2D [40]. An estimation of the mean cobalt crystallite size was obtained using the Scherrer formula [41] on the average FWHM. Pattern decomposition by Le Bail method [42] was applied with TOPAS v4.2 [43] software.

Fischer – Tropsch Synthesis

The activation procedure and FTS were performed in a 10 mm i.d. steel tube fixed-bed reactor. One gram of calcined catalyst was diluted with twenty parts per weight of SiC (75–150 μm), in order to reduce the temperature gradients throughout the catalyst bed. Aluminium blocks were fixed around the steel tube reactors to improve the heat distribution in the axial direction, and the reactors were placed in a furnace. Three thermocouples along the catalyst bed were used for temperature monitoring and control. Calcined catalyst followed a multistep activation procedure consisting of the following steps. A primary H_2 reduction (R) was performed at 350°C for 10 h with a ramping rate of 60 °C/h. The first reduction step was identical for all the samples. It is noted that the reference sample (REF) underwent only the first reduction step in H_2 before FTS. A carburization step (C) of the metallic nanoparticles followed. During carburization the reduced catalyst was exposed to pure CO (250 mL·min^{-1}·gcat^{-1}), at 230 °C. The reactor was first pressurized with Ar to 14 bar. [29] Then CO was introduced by replacing the Ar flow gradually, in order to keep the temperature increase in the catalyst bed below 2 °C during the carburization. Carburization lasted 3 hours with the exception of the 350^B catalyst that was exposed at 14 bar CO for 6 hours. Finally, prior to catalyst exposure at FTS conditions, a secondary H_2 reduction (R) was performed at different temperatures of 200 °C, 250 °C, 350 °C and 450 °C. The samples were treated with H_2 at 1 bar for 10 h with a ramping rate of 60 °C/h.

Fischer – Tropsch Synthesis was carried out in the same tubular fixed-bed reactor as activation for avoiding any exposure of the catalyst in air [29]. FTS was performed at 210 °C and 20 bar pressure with a H_2/CO ratio of 2.1. After the final activation step the catalyst was cooled to 170 °C and pressurized with He to 20 bar before the syngas feed of 250 Nml/min was introduced. Heating to the target temperature was done gradually. The sample was heated first to 190 °C with a ramping rate of 30 °C/h, then to 200 °C with a ramping rate of 5 °C/h, and finally to the target temperature of 210 °C with a ramp rate of ~6 °C/h. To collect wax and liquid products, one hot trap at ~85 °C and a cold trap at ambient temperature were used. Gas-phase products (after the traps) were fed into an HP 6890 gas chromatograph equipped with a thermal conductivity detector (TCD), and a flame ionization detector (FID). The synthesis gas contained 3% N_2, which served as an internal standard for quantification of the products. FTS was performed in two periods: Period A which is a period of 24 h time on stream (TOS) at a fixed space velocity and period B where the space velocity of the feed gas was adjusted to obtain 50 ± 5% CO conversion in order to record selectivity data at a fixed conversion level [22]. The selectivity data reported here are collected at similar conversion levels (46-48%) based on the analysis of C_1–C_4 hydrocarbons in the gas phase. Since the desired products are higher hydrocarbons, the selectivity is reported as C_{5+} and CH_4 selectivity.

Data analysis and interpretation

The selectivity results are discussed both in terms of absolute selectivities (C-atom based) and in terms of αC_n values (i.e. chain-growth probabilities of C_n^* intermediates on the catalyst surface). The αC_n values have been calculated according to the procedure reported elsewhere [44]. The αC_n values provide more comprehensive information regarding the FT mechanism, while the absolute selectivities are of more practical use. In the supporting information one can find a brief discussion on αC_n values interpretation based on the knowledge obtained from conventional Co-based catalysts, as well as detailed information on TOF calculations.

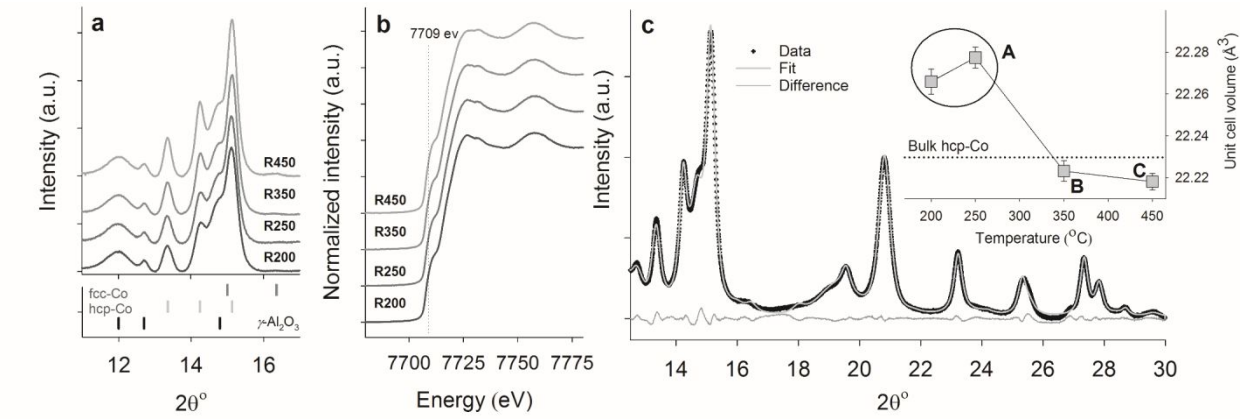

Figure 1. Diffraction and absorption X-ray signal of the activated catalytic materials *after H_2 reduction at 200 (R200), 250 (R250), 350 (R350) and 450°C (R450) (a) X-ray diffraction patterns obtained at 50°C (b) K-edge Co-XANES spectra measured during cooling (c) fit of the diffraction pattern for R450 together with volume (inset) of the unit cell obtained from Le Bail refinement against bulk hcp-Co (dotted line).*

3. Results and Discussion

The Co_2C/γ-Al_2O_3 precursor was decomposed at four different temperatures under H_2 atmosphere; 200°C (R200), 250°C (R250), 350°C ($R350^A$ and $R350^B$) and 450°C (R450). All four catalysts share similar properties (same support, similar crystallite sizes and extent of reduction, see later in text). The active catalysts were characterized and evaluated for their reaction performance at realistic FTS conditions (210 °C, 20 bar, H_2/CO ratio = 2.1, 50% CO conversion), Table 1. FTS performance for the four treatments differ significantly, taking into account the narrow range of the applied reduction temperatures and correspondingly small structural differences as visualized by synchrotron X-rays (Figure 1a). Apparently, all catalysts have relatively similar average crystallite sizes (Table 2), far from the size sensitivity regime (reported for *fcc*-Co NPs)[10]. In addition, all Co-XANES spectra of the reduced catalysts resemble bulk cobalt to a high degree (Figure 1b, Figure S1), meaning that a high reduction extent is achieved. Structural analysis at the nanoscale allows grouping of the catalysts in three categories. **The first category A** consists of the two catalysts R200 and R250, both reduced at moderate temperatures. The higher lattice volume of these two catalysts (Figure 1c) is probably due to the presence of carbon inside the lattice of the *hcp*-Co NPs. Refined *in situ* TPR-XRD data (Figure 2, Figure S2), show that in the temperature range up to 250 °C there is a shrinking unit cell and reduction in the d-spacing of the (013) *hcp*-Co reflection. The minimum at around 250 °C indicates that lattice carbon is removed at approximately this temperature. However, the relatively fast heating rate (3°C/min) and the dynamic nature of TPR analysis may lead to temperature deviations. In terms of catalytic performance, R200 and R250 catalysts exhibit signs of simultaneously high (low αC_1 and high CH_4 selectivity) and low hydrogenation activity (high olefin–to-paraffin ratios (o/p) for C_2 to C_6 hydrocarbons). In particular, the application of low reduction temperature gives more CH_4 and CO_2 than any other catalyst. Indeed, it has been shown that Co_2C species are stable under FTS conditions[45] giving higher selectivities to CH_4 and CO_2[46]. Apparently, there is similar FTS performance of the Co NPs with lattice carbon observed here and Co_2C. αC_1 and αC_4 probabilities show minimum values for these catalysts, as well as the C_{5+} selectivity (SC_{5+}). Reaction rates are at levels similar to that of the REF catalytic material. **Lattice carbon free Co crystallites, category B**, are obtained after H_2 reduction at 350°C ($R350^A$ and $R350^B$). Our previous thermogravimetric investigations on these carburized samples have shown negligible amount of carbon resistant to H_2 at 350°C [29]. From *in situ* XRD it can be concluded that all lattice carbon has been removed at this temperature as well. This is evident from the changes in unit cell volume, d_{013} and c/a ratio in Figure 2 and Figure S2. Furthermore, the Co surface area of the $R350^A$ is very close to that of the REF catalyst, with the dispersion (H_2 chemisorption) estimated to be 7.5% and 7.4%, respectively. The FTS performance in terms of activity and selectivity is however, exceptional. Particularly, in comparison with the REF catalyst the CO turnover rate is nearly doubled reaching 0.0903 s^{-1}, a value comparable to previously reported TOF value obtained at higher temperature (220°C) for a Pt promoted Co/γ-Al_2O_3 catalyst[28], when a similar RCR activation protocol was followed. Here it has to be noted that TOF values of structure sensitive reactions are indicative (see supporting information). The selectivity parameters are also influenced, with αC_2 to αC_4 values above 0.9, which are the highest values for all the γ-Al_2O_3 supported catalysts (Table 1), resulting in the highest SC_{5+}.

Table 1. ***FTS performance indicators****; reaction rate (r_{CO}), turn over frequency (TOF), product selectivities (C_{5+} , CH_4 , C_2-C_4 , CO_2), olefin–to-paraffin ratios (o/p) and chain growth probabilities of C_n* surface intermediates (αC_n, n = 1 - 4) for carbide decomposed at 200°C to 450°C together with conventional catalyst (REF, Co_3O_4 activated by H_2). FTS was performed at 210°C, 20 bar and H_2/CO ratio of 2.1. Reaction started at 15000 Nml/gcat and adjusted to give 50±1 % CO conversion after 24 h; selectivity C_{5+} was measured at 47±1 % CO conversion after approximately 48 h on stream. Hydrocarbon selectivities are reported on a CO_2-free basis.*

	r_{CO} mol CO·g$_{Cat}^{-1}$·h^{-1}	TOF s^{-1}	TOF XRD based, s^{-1}	C_{5+} C%	CH_4 C%	C_2-C_4 C%	CO_2 C%	o/p C_2	o/p C_3	o/p C_4	o/p C_5	o/p C_6	alpha αC_1	alpha αC_2	alpha αC_3	alpha αC_4
REF	0.044	0.049	0.062	82.1	8.6	9.3	0.18	0.10	2.32	1.38	1.09	0.73	0.543	0.956	0.865	0.869
R200	0.047		0.059	79.9	10.2	9.9	0.27	0.14	2.87	1.77	1.46	1.02	0.511	0.961	0.878	0.853
R250	0.046		0.058	81.1	9.8	9.1	0.22	0.15	3.07	1.92	1.70	1.25	0.513	0.962	0.880	0.862
R350^{A}	0.083	0.090	0.104	87.8	6.8	5.5	0.11	0.19	3.06	1.89	1.64	1.11	0.542	0.969	0.908	0.901
***R350^{B}**	0.088		0.110	88.3	6.6	5.0	0.11	0.22	3.31	2.09	1.84	1.33	0.539	0.972	0.914	0.904
R450	0.065		0.081	85.2	7.9	6.9	0.16	0.18	3.18	1.91	1.63	1.19	0.532	0.967	0.892	0.886

**$R350^{B}$ has a doubled carburization duration of 6 hours in comparison to other samples.*

αC_1, on the contrary, is similar to that of the reference catalyst. Another important observation is that the o/p ratios for C_2 to C_6 products are high, in particular the C_2 o/p ratio is about twice the value observed for the REF (around 0.2, compared to 0.098). CO_2 formation is suppressed with the lowest obtained values of all the samples tested.

The third category C, consists of catalyst R450 and is characterized by increase in the fraction of *fcc*-Co**.** Exposure of bulk *hcp*-Co to temperatures above ~420°C has been shown to initiate/trigger transformation to *fcc*-Co[47,48]. The topic is still a matter of scientific debate and various deviations from this transformation temperature have been reported and related to various factors such as NP size, metal-support interactions and pre-existing concentration of stacking faults[49–51]. Here, with *in situ* TPR-XRD, the transformation from *hcp*-Co to *fcc*-Co is followed. During the transition, atomic diffusion creates *fcc* domains and dislocations that lead to increased disorder that is visualized by changes in *c/a* (Figure 2) and d_{010} /d_{011} ratios (Figure S2), starting around 350°C in the TPR experiment. After the atomic relocations, and when adequate long-range order of *fcc*-Co forms, reflections of *fcc* planes become XRD visible. This is seen at temperatures above 470°C (Figure S2). Obviously, the phenomenon occurs in the bulk, however, secondary electron imaging studies on Co single crystals have shown that the transformation is initiated in the bulk and proceeds to the surface with a delay[52].

Table 2. *Size and degree of reduction (DOR) of the metallic Co NPs.*

	Crystallite size [nm]	Particle size** [nm]	DOR XANES [%]
Ref	13.2*	13.0 nm	-
R200	13.1	-	89±3
R250	13.5	-	92±3
R350	14.0	12.8 nm	95±3
R450	14.4	-	98±3

** from Co_3O_4 due to theoretical oxygen loss d(Co) = 0.8 × d(Co_3O_4).*
*** evaluated from H_2 chemisorption dispersion (D) measurements according to d(Co)=96.2/D%[36].*

In addition, transmission electron microscopy (TEM) studies on reduced Re/Co/γ-Al_2O_3 FTS catalysts activated by H_2 (containing *fcc-hcp* hybrid Co NPs) have shown a high concentrations of planar defects including twins, grain boundaries, edge dislocations, stacking faults and *hcp* lamellae in Co NPs[53].A similar observation has been obtained on fault-rich Cu NPs, where it was found that there is a high probability of termination of a twin boundary as a surface kink[9]. FTS performance indicators for the R450 catalyst are approaching the ones for the R350 catalysts, yet with reduced value of SC_{5+} and a substantial 26% decrease in the reaction rate compared to category B, despite the structural similarity (Figure 1 and Figure S2). The magnitude of the activity drop cannot be explained by the minor (3%) reduction in Co surface area due to sintering.

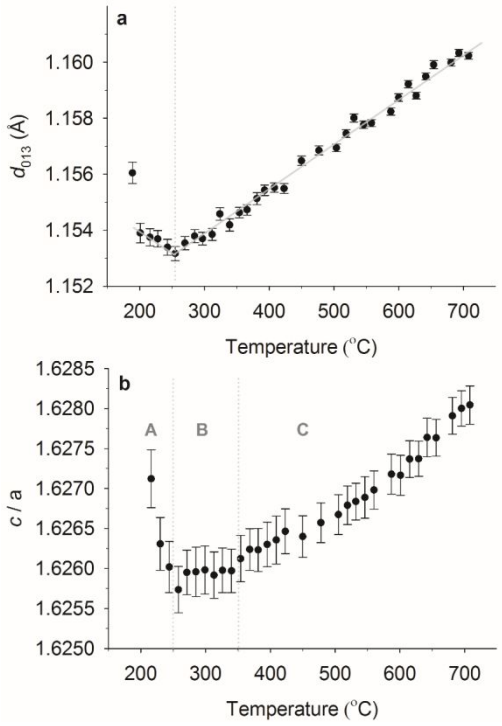

Figure 2. Structural evolution obtained from refinement of in situ TPR-XRD *(a) d spacing of 013 hcp-Co reflection and (b) c/a lattice parameters ratio from Le Bail refinement during TPR.*

Overall performance indicators (r_{CO}, SC_{5+}, o/p and chain growth probabilities αC_n) of the catalysts originating from the Co_2C precursor, show that the RCR protocol can potentially outperform conventional catalyst activation, provided that carbon is efficiently removed (Figure 3).

The reaction rates are at least equal to that of the REF catalytic material showing almost a doubling for the optimized category B catalysts, in spite of the very similar Co dispersion. The higher apparent CO turnover rates can be attributed to differences in electronic structure of the two Co polymorphs or to a larger number of active sites that can be accommodated. Regarding the electronic structure, DFT calculations have shown differences in the electron distribution density of the two phases[54], that might result in stronger CO adsorption over *hcp*-Co and subsequently higher reaction rates. Nevertheless, the most stable surfaces with highly coordinated Co atoms for the two polymorphs, i.e. *hcp*-Co (001) and *fcc*-Co (111), have the same surface geometry only differing in the third Co layer[55]. As such, electronic differences might have an impact only for less abundant surfaces. In terms of sites for CO dissociation, the size, the shape and phase of the NP dictate the number of B5 sites that are exposed (and/or *in situ* formed) capable of dissociating CO[56,57]. Theoretical molecular dynamic studies of *fcc*-Co and *hcp*-Co NPs have shown that differences between the two phases exist in terms of relative ratio of the exposed surfaces and the distribution of B5 sites. In particular, *hcp*-Co NPs have a slightly higher ratio of terraces to steps/kinks. Additionally, besides the common B5-A and B5-B sites, *hcp*-Co NPs show two more B5 site configurations with different properties (B5-B' and B5-C)[58]. A combination of the two might explain the differences in performance, however it should again be stressed that the theoretical calculated values on ideal NPs or model surfaces may significantly differ from the experimentally measured rates since Co NPs regularly exist in hybrid *fcc-hcp* structures. In addition to the reasons stated above, an enhancement of the rate could derive from changes in the proximity of preferential adsorption sites of surface species since it has been suggested that H, OH or H_2O are assisting the CO scission process[59–61] and therefore adjacency is needed. On a different perspective, if the reaction mechanism involves merely the highly coordinated surfaces[62] a less disrupted surface will as well be of benefit for the reaction.

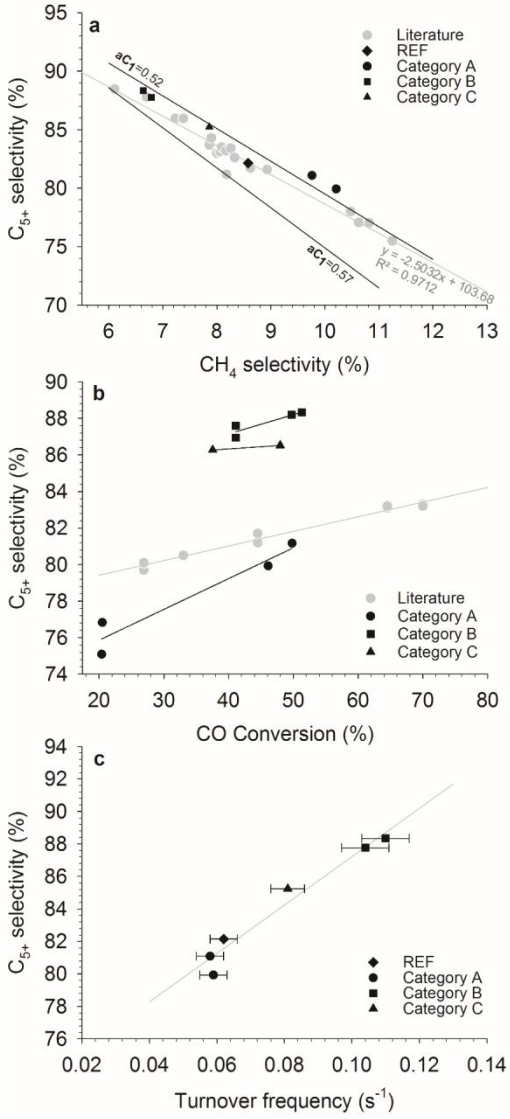

Figure 3. ***SC_{5+} related performance indicators in comparison with relevant literature.*** *Co and CoRe NPs prepared by IWI on γ-Al_2O_3, δ-Al_2O_3, ϑ-Al_2O_3 and α-Al_2O_3 at (210 °C, 20 bar, H_2/CO ratio of 2.1 and 47.5±2 % CO conversion) obtained from [22,63,64] and references therein.*

Selectivities to higher hydrocarbons of the category B and C catalysts deriving from the Co_2C precursor are comparable to selectivities that are achieved by less interacting and low surface area supports such as α-Al_2O_3, TiO_2 and partly SiO_2[44]. A comparison of the obtained data with respect to performance of conventionally prepared (i.e. by H_2 reduction of Co_3O_4 precursors) Al_2O_3 supported Co and CoRe NPs reported in the literature is presented in Figure 3. Figure 3c reveals a positive correlation between the apparent TOF (based on crystallite sizes obtained by XRD) and the higher αC_n values as well as SC_{5+} (Figure S3, Table S1). Similar correlations have been found for conventional catalysts[44] and suggest that the concentration of the monomer on the cobalt surface, the CH_x pool (ϑ_{CHx}),

dictates the higher αC_n values via a monomer surface-crowding mechanism[65]. Furthermore, the data from REF (higher αC_n values vs. TOF) fall more or less on the same trendlines, suggesting Co phase independent relationships. In addition, RCR catalysts show significantly lower αC_1 values (~0.52 – 0.57) compared to the higher αC_n values (>0.8) just as conventional Co-based FT catalysts do so [66,67]. These observations indicate that the mechanism(s) of forming methane and higher hydrocarbons are similar and in their essence irrespective of the crystalline phase of cobalt and based on a common CH_x monomer. Further support of the existence of a common monomer is found in the linear relationship between SC_{5+} and SC_1 (Figure 3a) that has been previously found for conventional Co-FTS catalysts [67]. Figure 3a compares the SC_{5+} vs. SC_1 values for the RCR catalysts with literature data for conventional catalysts with Co NPs > 6 nm at the same experimental conditions and conversion level. The scattering in the literature data is due to both experimental error ($\pm 2\sigma$, see supporting information) and actual differences in αC_1 ranging from 0.52 to 0.57[44]. Here, values from B and C category catalysts with the αC_1 values in the range (0.53 to 0.54) are following the trendline of the literature data, suggesting that the surface-crowding mechanism is valid. Exceptions are category A catalysts that with the lowest αC_1 (0.51) fall outside the range and drift upwards and will be discussed in more detail later.

For all RCR catalysts it is striking to see that **o/p ratios for C_2 to C_6 hydrocarbons** are reaching very high values (Figure 4a), higher than normally observed even with less interacting large-pore supports[31,44]. In particular, the R350 catalysts have twice as high C_2 o/p ratio compared to the REF, while the C_3 hydrocarbons at 47% CO conversion reach remarkable o/p values above 3, rarely seen in γ-Al_2O_3 supported catalysts[68] at such conversion levels and then only after H_2O addition [22,64] (Figure 4b). Since C_2 and C_3 o/p ratios are fair indicators of the relative hydrogen coverage (ϑ_H) on the cobalt surface[69], we propose that the catalysts with *hcp*-Co NPs have a lower ϑ_H than the conventionally activated catalyst. A further indication of this is seen in the relatively high αC_2 and αC_3 values of the category A catalysts. Despite having lower SC_{5+} and similar TOF as the REF, the αC_2 and αC_3 values are markedly higher than those of the REF. The connection between $\alpha C_2/\alpha C_3$ and ϑ_H is explained in Supporting Information.

Exceptions from the observed improved performance of the *hcp*-Co NPs are found for the **αC_1 values, which appear invariant**. On a big sample of selectivity data from conventional Co-based FT catalysts that share support and have been measured at identical process conditions, an inverse relationship between higher αC_n values (n > 1) and αC_1 has been found[44]. Here, comparing with the FT results of the REF catalyst it is apparent that the change from fcc rich hybrid *fcc/hcp*-Co to *hcp*-Co NPs increases most performance indicators (i.e. αC_{2+} and TOF), while αC_1 is invariant (the exception is category A catalysts that exhibit a reduction in αC_1). The fact that αC_1 does not follow an inverse relationship with higher αC_n values, but rather stays the same, could possibly be explained by a counteracting effect of a lowered ϑ_H.

Figure 3b shows the **effect of conversion level** on SC_{5+}. It appears that indigenous $H_2O_{(g)}$ has a stronger positive influence on SC_{5+} for the catalysts reduced at moderate temperatures (Category A), when compared with literature values[22,63]. αC_1 to αC_4 chain growth probabilities on these catalysts increase significantly at higher conversions (Table 2S). From the above and the observed reduction in CO_2 production with time on stream (Figure S4) a partial removal of carbon by H_2O could be assumed.

Comparison between RCR produced catalysts. **Category A** catalysts exhibit poor FTS performance regarding selectivity. DFT calculations have shown that subsurface carbon modifies the electronic structure of the Co surface[55]. Lattice carbon residues appear to interact and alter the properties of the Co surface resulting in a surface with the lowest αC_1 and αC_4 probabilities. The low αC_4 can be related to the lower apparent TOF, compared to the other RCR catalysts, resulting in a lower coverage of CH_x. The αC_1 is the single chain growth probability that is most affected by: changes in operating conditions [67,69,70], the presence of mass transfer limitations on reactant arrival[71], and the presence of "pure methanation" sites[67]. A high ϑ_H, mass transfer limitations and "pure methanation" sites would generally result in a lowered αC_1. All catalysts in the present study have particle size less than 90 µm and are subjected to identical conditions. In addition, judging from their high o/p ratios and high αC_2 and αC_3 values, high ϑ_H does not seem probable. Instead, "pure methanation" sites can be postulated and are indeed supported by the high CH_4 selectivity as compared with the reference material at very similar rates (Figure 3a). We propose that the existence of strong primary hydrogenation function is rather localized (few sites producing methane at high rates) since these catalysts retain high o/p ratios.

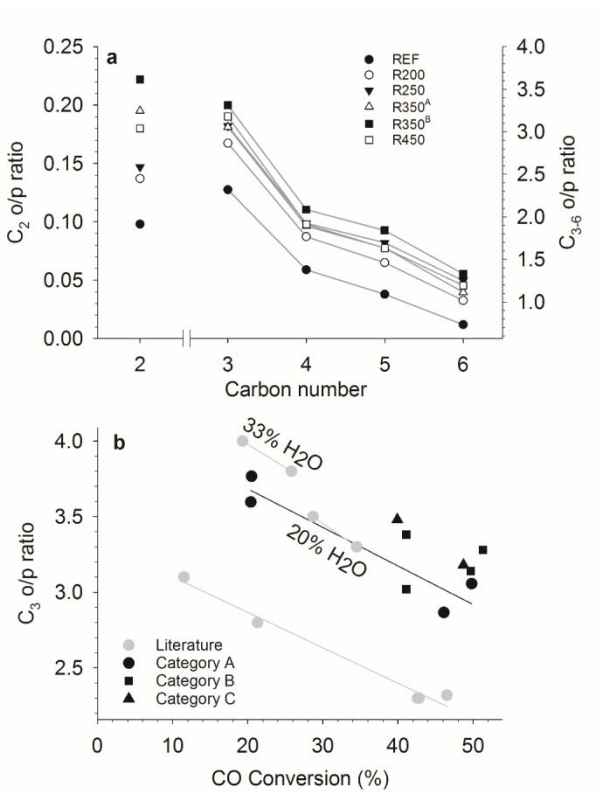

Figure 4. ***Olefin-to-paraffin ratio related performance indicators.*** *Comparison with relevant literature of Co and CoRe NPs prepared by IWI on γ-Al_2O_3, δ-Al_2O_3, ϑ-Al_2O_3 and α-Al_2O_3 at (210 °C, 20 bar, H_2/CO ratio of 2.1 and 47.5±2 % CO conversion) obtained from* [22,63,64] *and references therein*.

The **B category** catalysts outperform the other tested materials in all performance indicators (Table 1) and can be compared with the superior performance of α-Al_2O_3 and TiO_2 supported Co NPs[44]. Following this pretreatment, the Co crystallites are rich in *hcp*-Co, with indications of stacking disorder and small contributions from *fcc*-Co (Figure S2). We propose that these materials possess minimum disorder of all the tested samples (Figure 2). The higher turnover rates achieved allow a significant increase in space velocity and consequently lower bed residence times, which result in minimization of secondary reactions[16]. In accordance, the relative CO_2 formation is at a minimum, demonstrating further suppression of the secondary water-gas-shift reaction.

Category C; the R450 catalyst shows an increase in lattice disorder due to initiation of phase transformation and increase in the *fcc* concentration. This structural change, although small, is accompanied by a significant drop in reaction rate, corresponding to a reduction in the amount and/or reactivity of sites that can dissociate CO. A decrease in selectivity indicators is also apparent.

Previous TEM studies on similar catalysts demonstrated that stacking faults appear to terminate in the surface of the nanoparticle as coordinatively unsaturated sites (cus) at edges and steps[53]. In fact, even without termination to a cus the creation of lattice mismatch leads to the creation of strained overlayers and thus more reactive (in terms of adsorption/dissociation) sites due to change in the d-band induced by stress[6]. This implies that the stacking disorder seen in the bulk may negatively influence sites in the surface of the Co NP. We interpret the present results of increased lattice disorder coupled with a reduction in reaction rate as a structure sensitivity issue, where high concentration of cus has a negative effect on activity and selectivity in an analogue way to the particle size sensitivity described by den Breejen *et al.*[72]. We speculate that part of the additionally formed cus is poisoned by strong CO adsorption while a portion is providing H_2 dissociation increasing ϑ_H. The additional supply of H is expected to negatively affect the propagation rates as seen in αC_2 and αC_3 for the R450 catalyst. Furthermore, creation of planar defects may divide the NP in such a way that mobility of the CH_x monomer is hindered. Previous STM studies have shown that Co surface reconstructs under syngas exposure[56,73]. In light of recent data from *in situ* STM the importance of terraces is highlighted[74,75] particularly for their ability to form nano-islands and therefore their ability to provide additional step sites capable of CO dissociation. Provided that stacking faults formed during the *fcc* transition are terminated as cus, terrace sites will be disrupted rendering the surface unable to reconstruct forming nano-islands to the same extent. Inhibition of surface reconstruction has been found on Co surfaces after ppm alkali addition[76] that results in reaction rate loss in similar levels to the current study.

An un-promoted Co/α-Al_2O_3 responded with a performance enhancement when an identical RCR activation procedure was followed (Table 3), especially with regard to selectivity. Although the activity and αC_1 practically remain on the same levels after treatment and o/p ratios are not boosted in comparable levels to the γ-Al_2O_3 analogue, a similar boost in SC_{5+} (7%) and C_3 o/p ratio (10%) is apparent followed by a slight increase in higher alpha values (αC_{2+}) (Figure 6S). Similarly to the γ-Al_2O_3 analogue, suppression of the CH_4 and CO_2 is also observed (Figure S6).

Table 3. ***FTS performance indicators for unpromoted α-Al_2O_3 supported catalyst****; reaction rate r_{CO}, product selectivities, olefin–to-paraffin ratios (o/p) and chain growth probabilities of C_n* surface intermediates (αC_n, n = 1 – 4) for carbide decomposed at 350 °C and conventional catalyst (α-REF, Co_3O_4 activated by H_2). FTS was performed at 210°C, 20 bar and H_2/CO ratio of 2.1. Reaction started at 14500 Nml/gcat and adjusted to give 30±1 % CO conversion after 24 h; selectivity C_{5+} was measured at 28±1 % CO conversion). Hydrocarbon selectivities are reported on a CO_2-free basis.*

Co/α-Al_2O_3	r_{CO}	C_{5+}	CH_4	C_2-C_4	CO_2	o/p					alpha			
	mol CO / g Cat*h	C%	C%	C%	C%	C_2	C_3	C_4	C_5	C_6	αC_1	αC_2	αC_3	αC_4
α-REF	0.0066	81.9	7.9	10.2	0.52	0.13	2.66	1.71	1.55	1.32	0.572	0.933	0.849	0.871
α-R350	0.0070	88.0	6.3	5.7	0.41	0.17	2.92	1.93	1.85	1.45	0.560	0.953	0.893	0.906

It has to be noted that carbon diffusion during carburization and/or reduction steps of the RCR protocol might exhibit a size sensitivity and therefore the formed Co_2C on α-Al_2O_3 may not be as crystalline, or more stable carbon is produced not allowing a full utilization. Nevertheless, the selectivity enhancement is demonstrated and provides evidence for the significance of the NP phase on the FTS performance, suggesting that impact of support and promoter are of a secondary nature. Our data on the unpromoted Co/α-Al_2O_3 catalyst demonstrates the relevance and universality of our results to other systems. More importantly, the presented structural modification of Co NPs towards defect free nano-crystallites with maximum FTS performance could be applied on high surface area and highly interacting porous supports giving two major advantages: (a) The inhibition of NP sintering, the primary deactivation cause, through maximization of interparticle distances[77] and metal-support interaction (b) Formulation of catalysts with high Co loadings for maximizing catalyst productivity, minimizing process volume and potentially facilitating intensified process applications[16,78].

4. Conclusions

In our approach we decouple the microstructure of (Re promoted) Co NPs from other structural parameters that affect FT catalysis (particle size, support, porous network) through an RCR activation protocol. This protocol delivers a simpler, in terms of crystal purity, model catalyst allowing the study of minor differences at the Co nanoparticle level due to the simplification of the crystal structure to predominantly *hcp* compared to the complex intensely intergrown system seen after H_2 activation of Co oxides. In summary our findings indicate that:

- Al_2O_3 supported *hcp*-Co NPs outperform the highly faulted *fcc*-Co NPs commonly obtained by H_2 reduction, in agreement with previous studies. Yet there is a narrow window of utilization of the benefits that lays between carbon removal (>250°C) and initiation of stacking disorder (<450°C).
- The catalyst with highest concentration of *hcp*-Co and minimum number of defects, has the highest TOF and, accordingly, the highest SC_{5+} and chain-growth probability (αC_{2+}). This is ascribed to a higher population of CH_x that might derive from a higher intrinsic activity or accommodation of higher number of active sites.
- Apparently, chain growth over Co NPs follows a CH_x monomer surface-crowding mechanism independently of the nanoparticle crystalline phase, with evidenced, to a first approximation, relationships between higher αC_n and TOF.
- The exposed Co surfaces on *hcp*-Co NPs seem to have a lower relative hydrogen coverage ϑ_H than their highly faulted *fcc*-Co counterparts, resulting in higher o/p ratios and in lower relative termination rates of C_{2*} - C_{3*} surface intermediates.
- Residual carbon from the carburization step is present in the lattice of Co NPs with final reduction temperature lower than 350°C (R200 and R250). This lattice carbon significantly increases the methanation function of the catalysts as visualized from changes in αC_1 and selectivity toward CH_4.
- Structural faults have a negative impact on SC_{5+} and TOF. The results point to an enhanced capacity of the CH_x pool on the defect free *hcp*-Co NP surface, possibly by allowing reconstruction and formation of sites highly active for CO dissociation. Suppression of H supplied from cus may explain part of the increased relative propagation rates of lower carbon number surface intermediates.

Apparently, the size sensitivity of the FTS has to be re-established with respect to Co phase and faults. Our results pave the way for Co based FTS catalyst design

with optimized activity and selectivity to higher hydrocarbons through avoidance of microstructural defects. With the optimized Co NPs it is possible to achieve high SC_{5+} with a high productivity per gram catalyst on high interacting/high surface area supports that allow higher Co loadings to be obtained and simultaneous reduction of sintering rates.

Supporting Information

A more detailed description on the basis of the interpretation of the chain growth probabilities of the Cn* surface intermediates (the αC_n values) together with figures on structural similarity, structural changes during TPR, TOF, change of performance indicators from period of similar GHSW to similar conversion level, comparison of RCR response on $Re/Co/Al_2O_3$ and Co/Al_2O_3 and deactivation with time on stream are given in supporting information.

Acknowledgements

The project is funded by Research Council of Norway and Statoil under the GASSMAKS research program (grant no. 215519/E30). ESRF personnel at SNBL-BM01B are highly acknowledged for experimental assistance.

References

(1) Boudart, M. Catalysis by Supported Metals. In *Catal Rev*; 1969; pp 153–166.

(2) Gates, B. C. Supported Metal Clusters: Synthesis, Structure, and Catalysis. *Chem. Rev.* **1995**, *95*, 511–522.

(3) Somorjai, G. A.; Carrazza, J. Structure Sensitivity of Catalytic Reactions. *Ind. Eng. Chem. Fundam.* **1986**, *25*, 63–69.

(4) Bell, A. T. The Impact of Nanoscience on Heterogeneous Catalysis. *Science* **2003**, *299*, 1688–1691.

(5) Nørskov, J. K.; Abild-Pedersen, F.; Studt, F.; Bligaard, T. Density Functional Theory in Surface Chemistry and Catalysis. *Proc. Natl. Acad. Sci.* **2011**, *108*, 937–943.

(6) Mavrikakis, M.; Hammer, B.; Nørskov, J. K. Effect of Strain on the Reactivity of Metal Surfaces. *Phys. Rev. Lett.* **1998**, 2819–2822.

(7) Somorjai, G. A. Modern Surface Science and Surface Technologies: An Introduction. *Chem. Rev.* **1996**, *96*, 1223–1236.

(8) Kandemir, T.; Girgsdies, F.; Hansen, T. C.; Liss, K. D.; Kasatkin, I.; Kunkes, E. L.; Wowsnick, G.; Jacobsen, N.; Schlögl, R.; Behrens, M. InSitu Study of Catalytic Processes: Neutron Diffraction of a Methanol Synthesis Catalyst at Industrially Relevant Pressure. *Angew. Chem. Int. Ed. Engl.* **2013**, *52*, 5166–5170.

(9) Behrens, M.; Studt, F.; Kasatkin, I.; Kuhl, S.; Havecker, M.; Abild-Pedersen, F.; Zander, S.; Girgsdies, F.; Kurr, P.; Kniep, B.-L.; Tovar, M.; Fischer, R. W.; Nørskov, J. K.; Schlögl R. The Active Site of Methanol Synthesis over Cu/ZnO/Al2O3 Industrial Catalysts. *Science* **2012**, *336*, 893–897.

(10) Bezemer, G. L. L.; Bitter, J. H.; Kuipers, H. P. C. E.; Oosterbeek, H.; Holewijn, J. E.; Xu, X.; Kapteijn, F.; van Dillen, A. J.; de Jong, K. P. Cobalt Particle Size Effects in the Fischer-Tropsch Reaction Studied with Carbon Nanofiber Supported Catalysts. *J. Am. Chem. Soc.* **2006**, *128*, 3956–3964.

(11) Fischer, F.; Tropsch, H. The Synthesis of Petroleum at Atmospheric Pressures from Gasification Products of Coal. *Brennst.-Chem.* **1926**, *7*, 97.

(12) Khodakov, A. Y.; Chu, W.; Fongarland, P. Advances in the Development of Novel Cobalt Fischer-Tropsch Catalysts for Synthesis of Long-Chain Hydrocarbons and Clean Fuels. *Chem. Rev.* **2007**, *107*, 1692–1744.

(13) Marxer, D.; Furler, P.; Scheffe, J.; Geerlings, H.; Falter, C.; Batteiger, V.; Sizmann, A.; Steinfeld, A. Demonstration of the Entire Production Chain to Renewable Kerosene via Solar Thermochemical Splitting of H 2 O and CO 2. *Energy & Fuels* **2015**, *29*, 3241–3250.

(14) Hofer, L. J. E.; Peebles, W. C. X-Ray Diffraction Studies of the Action of Carbon Monoxide on Cobalt-Thoria-Kieselguhr Catalysts. I 1. *J. Am. Chem. Soc.* **1947**, *69*, 2497–2500.

(15) Colley, S. E.; Copperthwaite, R. G.; Hutchings, G. J.; Terblanche, S. P.; Thackeray, M. M. Identification of Body-Centred Cubic Cobalt and Its Importance in CO Hydrogenation. *Nature* **1989**, *339*, 129–130.

(16) Iglesia, E. Design, Synthesis, and Use of Cobalt-Based Fischer-Tropsch Synthesis Catalysts. *Appl. Catal. A Gen.* **1997**, *161*, 59–78.

(17) Geerlings, J. J. C.; Zonnevylle, M. C.; de Groot, C. P. M. Structure Sensitivity of the Fischer-Tropsch Reaction on Cobalt Single Crystals. *Surf. Sci.* **1991**, *241*, 315–324.

(18) Barbier, A.; Tuel, A.; Arcon, I.; Kodre, A.; Martin, G. A. Characterization and Catalytic Behavior of Co / SiO 2 Catalysts : Influence of Dispersion in the Fischer – Tropsch Reaction. *J. Catal.* **2001**, *116*, 106–116.

(19) den Breejen, J. P.; Radstake, P. B.; Bezemer, G. L. L.; Bitter, J. H.; Frøseth, V.; Holmen, A.; De Jong, K. P. On the Origin of the Cobalt Particle Size Effects in Fischer-Tropsch Catalysis. *J. Am. Chem. Soc.* **2009**, *131*, 7197–7203.

(20) Prieto, G.; Martínez, A.; Concepción, P.; Moreno-Tost, R. Cobalt Particle Size Effects in Fischer – Tropsch Synthesis : Structural and in Situ Spectroscopic Characterisation on Reverse Micelle-Synthesised Co / ITQ-2 Model Catalysts. *J. Catal.* **2009**, *266*, 129–144.

(21) Borg, Ø.; Dietzel, P. D. C.; Spjelkavik, A. I.; Tveten, E. Z.; Walmsley, J. C.; Diplas, S.; Eri, S.; Holmen, A.; Rytter, E. Fischer–Tropsch Synthesis: Cobalt Particle Size and Support Effects on Intrinsic Activity and Product Distribution. *J. Catal.* **2008**, *259*, 161–164.

(22) Rytter, E.; Tsakoumis, N. E.; Holmen, A. On the Selectivity to Higher Hydrocarbons in Co-Based Fischer–Tropsch Synthesis. *Catal. Today* **2016**, *261*, 3–16.

(23) Tsakoumis, N. E.; Walmsley, J. C.; Rønning, M.; van Beek, W.; Rytter, E.; Holmen, A. Evaluation of Reoxidation Thresholds for γ-Al 2 O 3 -Supported

Cobalt Catalysts under Fischer–Tropsch Synthesis Conditions. *J. Am. Chem. Soc.* **2017**, *139*, 3706–3715.

(24) Dinega, D. P.; Bawendi, M. G. A Solution-Phase Chemical Approach to a New Crystal Structure of Cobalt. *Angew. Chem. Int. Ed. Engl.* **1999**, *38*, 1788–1791.

(25) Ducreux, O.; Rebours, B.; Lynch, J.; Roy-Auberger, M.; Bazin, D. Microstructure of Supported Cobalt Fischer-Tropsch Catalysts. *Oil Gas Sci. Technol. - Rev. l'IFP* **2008**, *64*, 49–62.

(26) Rebmann, E.; Fongarland, P.; Lecocq, V.; Diehl, F.; Schuurman, Y. Kinetic Modeling of Transient Fischer–Tropsch Experiments over Co/Al2O3 Catalysts with Different Microstructures. *Catal. Today* **2016**, *20*, 207–209.

(27) Liu, J.-X.; Su, H.-Y.; Sun, D.-P.; Zhang, B.-Y.; Li, W.-X. Crystallographic Dependence of CO Activation on Cobalt Catalysts: HCP versus FCC. *J. Am. Chem. Soc.* **2013**, *135*, 16284–16287.

(28) Karaca, H.; Safonova, O. V.; Chambrey, S.; Fongarland, P.; Roussel, P.; Griboval-Constant, A.; Lacroix, M.; Khodakov, A. Y. Structure and Catalytic Performance of Pt-Promoted Alumina-Supported Cobalt Catalysts under Realistic Conditions of Fischer–Tropsch Synthesis. *J. Catal.* **2011**, *277*, 14–26.

(29) Patanou, E.; Tsakoumis, N. E.; Myrstad, R.; Blekkan, E. A. The Impact of Sequential H 2 -CO-H 2 Activation Treatment on the Structure and Performance of Cobalt Based Catalysts for the Fischer-Tropsch Synthesis. *Appl. Catal. A Gen.* **2018**, *549*, 280–288.

(30) Prieto, G.; De Mello, M. I. S.; Concepción, P.; Murciano, R.; Pergher, S. B. C.; Martínez, A. Cobalt-Catalyzed Fischer–Tropsch Synthesis: Chemical Nature of the Oxide Support as a Performance Descriptor. *ACS Catal.* **2015**, *5*, 3323–3335.

(31) Borg, Ø.; Eri, S.; Blekkan, E. A.; Storsæter, S.; Wigum, H.; Rytter, E.; Holmen, A. Fischer-Tropsch Synthesis over γ-Alumina-Supported Cobalt Catalysts: Effect of Support Variables. *J. Catal.* **2007**, *248*, 89–100.

(32) Saib, A. M.; Claeys, M.; van Steen, E. Silica Supported Cobalt Fischer–Tropsch Catalysts: Effect of Pore Diameter of Support. *Catal. Today* **2002**, *71*, 395–402.

(33) Rytter, E.; Holmen, A. On the Support in Cobalt Fischer–Tropsch Synthesis—Emphasis on Alumina and Aluminates. *Catal. Today* **2016**, *275*, 11–19.

(34) Tsakoumis, N. E.; Voronov, A.; Rønning, M.; Beek, W. Van; Borg, Ø.; Rytter, E.; Holmen, A. Fischer–Tropsch Synthesis: An XAS/XRPD Combined in Situ Study from Catalyst Activation to Deactivation. *J. Catal.* **2012**, *291*, 138–148.

(35) Dehghan-Niri, R.; Hansen, T. W.; Wagner, J. B.; Holmen, A.; Rytter, E.; Borg, Ø.; Walmsley, J. C. In-Situ Reduction of Promoted Cobalt Oxide Supported on Alumina by Environmental Transmission Electron Microscopy. *Catal. Letters* **2011**, *141*, 754–761.

(36) Reuel, R. C.; Bartholomew, C. H. The Stoichiometries of H2 and CO Adsorptions on Cobalt: Effects of Support and Preparation. *J. Catal.* **1984**, *85*, 63–77.

(37) Diehl, F.; Khodakov, A. Y. Promotion of Cobalt Fischer-Tropsch Catalysts with Noble Metals: A Review. *Oil Gas Sci. Technol. - Rev. l'IFP* **2008**, *64*, 11–24.

(38) Rønning, M.; Tsakoumis, N. E.; Voronov, A.; Johnsen, R.; Norby, P.; Beek, W. Van; Borg, Ø.; Rytter, E.; Holmen, A. *Combined XRD and XANES studies of a Re-promoted Co/γ-Al_2O_3 catalyst at Fischer–Tropsch synthesis conditions. Catal. Today* **2010**, 155, 289-295.

(39) Ravel, B.; Newville, M. ATHENA , ARTEMIS , HEPHAESTUS : Data Analysis for X-Ray Absorption Spectroscopy Using IFEFFIT. *J. Synchrotron Radiat.* **2005**, *12*, 537–541.

(40) Hammersley, A. P.; Svensson, S. O.; Hanfland, M.; Fitch, A. N.; Hausermann, D. Two-Dimensional Detector Software: From Real Detector to Idealised Image or Two-Theta Scan. *High Pressure Research*. 1996, pp 235–248.

(41) Scherrer, P. Estimation of the Size and Internal Structure of Colloidal Particles by Means of Röntgen Rays. *Gottingen Nachrichten* **1918**, *2*, 98.

(42) Pawley, G. S. Unit-Cell Refinement from Powder Diffraction Scans. *J. Appl. Crystallogr.* **1981**, *14*, 357–361.

(43) Coelho, A. General Profile and Structure Analysis Software for Powder Diffraction Data. - User's Manual. **2008**, Topas V4.2 (Bruker AXS), Karlsruhe, Germany.

(44) Lögdberg, S.; Yang, J.; Lualdi, M.; Walmsley, J. C.; Järås, S.; Boutonnet, M.; Blekkan, E. A.; Rytter, E.; Holmen, A. Further Insights into Methane and Higher Hydrocarbons Formation over Cobalt-Based Catalysts with γ-Al 2 O 3 , α-Al 2 O 3 and TiO 2 as Support Materials. *J. Catal.* **2017**, *352*, 515–531.

(45) Claeys, M.; Dry, M. E.; van Steen, E.; du Plessis, H. E.; Van Berge, P. J.; Saib, A. M.; Moodley, D. J. In Situ Magnetometer Study on the Formation and Stability of Cobalt Carbide in Fischer–Tropsch Synthesis. *J. Catal.* **2014**, *318*, 193–202.

(46) Mohandas, J. C.; Gnanamani, M. K.; Jacobs, G.; Ma, W.; Ji, Y.; Khalid, S.; Davis, B. H. Fischer–Tropsch Synthesis: Characterization and Reaction Testing of Cobalt Carbide. *ACS Catal.* **2011**, *1*, 1581–1588.

(47) Kitakami, O.; Sato, H.; Shimada, Y.; Sato, F.; Tanaka, M. Size Effect on the Crystal Phase of Cobalt Fine Particles. *Phys. Rev. B* **1997**, *56*, 13849–13854.

(48) Houska, C. R.; Averbach, B. L.; Cohen, M. The Cobalt Transformation. *Acta Metall.* **1960**, *8*, 81–87.

(49) Andreev, A. S.; d'Espinose de Lacaillerie, J.-B.; Lapina, O. B.; Gerashenko, A. Thermal Stability and Hcp-Fcc Allotropic Transformation in Supported Co Metal Catalysts Probed near Operando by Ferromagnetic NMR. *Phys. Chem. Chem. Phys.* **2015**, *17*, 14598–14604.

(50) Tsakoumis, N. E.; Dehghan-Niri, R.; Johnsen, R. E.; Voronov, A.; van Beek, W.; Walmsley, J. C.; Borg, Ø.; Rytter, E.; Chen, D.; Rønning, M.; Holmen, A. A Combined in Situ XAS-XRPD-Raman Study of Fischer–Tropsch Synthesis over a Carbon Supported Co Catalyst. *Catal. Today* **2013**, *205*, 86–93.

(51) Tsakoumis, N. E.; Johnsen, R. E.; van Beek, W.; Rønning, M.; Rytter, E.; Holmen, A. Capturing Metal-Support Interactions in Situ during the Reduction of a Re Promoted Co/γ-Al2O3 Catalyst. *Chem. Commun.* **2016**, *52*, 3239–3242.

(52) Erbudak, M.; Wetli, E.; Hochstrasser, M.; Pescia, D.; Vvedensky, D. D. Surface Phase Transitions during Martensitic Transformations of Single-Crystal Co. *Phys. Rev. Lett.* **1997**, *79*, 1893–1896.

(53) Dehghan-Niri, R. *Advanced Transmission Electron Microscopy Studies of Cobalt Fischer-Tropsch Catalysts*; NTNU: PhD-thesis, 2012.

(54) de la Peña O'Shea, V. A.; Moreira, I. D. P. R.; Roldán, A.; Illas, F. Electronic and Magnetic Structure of Bulk Cobalt: The Alpha, Beta, and Epsilon-Phases from Density Functional Theory Calculations. *J. Chem. Phys.* **2010**, *133*, 024701.

(55) Van Helden, P.; Ciobîcă, I. M. A DFT Study of Carbon in the Subsurface Layer of Cobalt Surfaces. *ChemPhysChem* **2011**, *12*, 2925–2928.

(56) Wilson, J. H.; de Groot, C. Atomic-Scale Restructuring in High-Pressure Catalysis. *J. Phys. Chem.* **1995**, *99*, 7860–7866.

(57) van Helden, P.; Ciobîcă, I. M.; Coetzer, R. L. J. The Size-Dependent Site Composition of FCC Cobalt Nanocrystals. *Catal. Today* **2016**, *261*, 48–59.

(58) Agrawal, R.; Phatak, P.; Spanu, L. Effect of Phase and Size on Surface Sites in Cobalt Nanoparticles. *Catal. Today* **2018**.

(59) Storsæter, S.; Chen, D.; Holmen, A. Microkinetic Modelling of the Formation of C1 and C2 Products in the Fischer-Tropsch Synthesis over Cobalt Catalysts. *Surf. Sci.* **2006**, *600*, 2051–2063.

(60) Hibbitts, D. D.; Loveless, B. T.; Neurock, M.; Iglesia, E. Mechanistic Role of Water on the Rate and Selectivity of Fischer-Tropsch Synthesis on Ruthenium Catalysts. *Angew. Chem. Int. Ed. Engl.* **2013**, *52*, 12273–12278.

(61) Rytter, E.; Holmen, A. Consorted Vinylene Mechanism for Cobalt Fischer–Tropsch Synthesis Encompassing Water or Hydroxyl Assisted CO-Activation. *Top. Catal.* **2018**, *61*, 1024–1034.

(62) Ojeda, M. P.; Nabar, R.; Nilekar, A. U.; Ishikawa, A.; Mavrikakis, M.; Iglesia, E. CO Activation Pathways and the Mechanism of Fischer – Tropsch Synthesis. *J. Catal.* **2010**, *272*, 287–297.

(63) Rytter, E.; Holmen, A. Perspectives on the Effect of Water in Cobalt Fischer-Tropsch Synthesis. *ACS Catal.* **2017**, *7*, 5321–5328.

(64) Storsæter, S.; Borg; Blekkan, E. A.; Holmen, A. Study of the Effect of Water on Fischer-Tropsch Synthesis over Supported Cobalt Catalysts. *J. Catal.* **2005**, *231*, 405–419.

(65) Mims, C. A.; Bertole, C. J. Surface Carbon Coverage and Selectivity in FT Synthesis: A Simple Model for Selectivity Correlations. *Stud. Surf. Sci. Catal.* **2001**, *Volume 136*, 375–380.

(66) Iglesia, E.; Reyes, S. C.; Madon, R. J.; Soled, S. L. Selectivity Control and Catalyst Design in the Fischer-Tropsch Synthesis: Sites, Pellets, and Reactors; 1993; pp 221–302.

(67) Lögdberg, S.; Lualdi, M.; Järås, S.; Walmsley, J. C.; Blekkan, E. A.; Rytter, E.; Holmen, A. On the Selectivity of Cobalt-Based Fischer–Tropsch Catalysts: Evidence for a Common Precursor for Methane and Long-Chain Hydrocarbons. *J. Catal.* **2010**, *274*, 84–98.

(68) Duyckaerts, N.; Bartsch, M.; Trotuş, I.-T.; Pfänder, N.; Lorke, A.; Schüth, F.; Prieto, G. Intermediate Product Regulation in Tandem Solid Catalysts with Multimodal Porosity for High-Yield Synthetic Fuel Production. *Angew. Chemie Int. Ed.* **2017**, *56*, 11480–11484.

(69) Bertole, C. J.; Kiss, G.; Mims, C. A. The Effect of Surface-Active Carbon on Hydrocarbon Selectivity in the Cobalt-Catalyzed Fischer-Tropsch Synthesis. *J. Catal.* **2004**, *223*, 309–318.

(70) Todic, B.; Ma, W.; Jacobs, G.; Davis, B. H.; Bukur, D. B. Effect of Process Conditions on the Product Distribution of Fischer-Tropsch Synthesis over a Re-Promoted Cobalt-Alumina Catalyst Using a Stirred Tank Slurry Reactor. *J. Catal.* **2014**, *311*, 325–338.

(71) Lualdi, M.; Lögdberg, S.; Di Carlo, G.; Järås, S.; Boutonnet, M.; Venezia, A. M.; Blekkan, E. A.; Holmen, A. Evidence for Diffusion-Controlled Hydrocarbon Selectivities in the Fischer-Tropsch Synthesis over Cobalt Supported on Ordered Mesoporous Silica. *Top. Catal.* **2011**, *54*, 1175–1184.

(72) den Breejen, J. P.; Radstake, P. B.; Bezemer, G. L. L.; Bitter, J. H.; Frøseth, V.; Holmen, A.; Jong, K. P. De. On the Origin of the Cobalt Particle Size Effects in Fischer−Tropsch Catalysis. *J. Am. Chem. Soc.* **2009**, *131*, 7197–7203.

(73) Venvik, H. J.; Borg, A.; Berg, C. Formation of the CO-Induced (3 x 1) Surface Structure on Co (1150) Studied by STM. *Surf. Sci.* **1998**, *397*, 322–332.

(74) Navarro, V.; van Spronsen, M. A.; Frenken, J. W. M. In Situ Observation of Self-Assembled Hydrocarbon Fischer–Tropsch Products on a Cobalt Catalyst. *Nat. Chem.* **2016**, *8*, 929–934.

(75) Banerjee, A.; Navarro, V.; Frenken, J. W. M.; Van Bavel, A. P.; Kuipers, H. P. C. E.; Saeys, M. Shape and Size of Cobalt Nanoislands Formed Spontaneously on Cobalt Terraces during Fischer-Tropsch Synthesis. *J. Phys. Chem. Lett.* **2016**, *7*, 1996–2001.

(76) Strømsheim, M. D.; Svenum, I. H.; Farstad, M. H.; Li, Z.; Gavrilovic, L.; Guo, X.; Lervold, S.; Borg, A.; Venvik, H. J. Effects of K Adsorption on the CO-Induced Restructuring of Co(11-20). *Catal. Today* **2018**, *299*, 37–46.

(77) Prieto, G.; Zečević, J.; Friedrich, H.; de Jong, K. P.; de Jongh, P. E.; Jong, K. P. De; Jongh, P. E. De. Towards Stable Catalysts by Controlling Collective Properties of Supported Metal Nanoparticles. *Nat. Mater.* **2012**, *12*, 34–39.

(78) Sun, X.; Suarez, A. I. O.; Meijerink, M.; van Deelen, T.; Ould-Chikh, S.; Zečević, J.; de Jong, K. P.; Kapteijn, F.; Gascon, J. Manufacture of Highly Loaded Silica-Supported Cobalt Fischer–Tropsch Catalysts from a Metal Organic Framework. *Nat. Commun.* **2017**, *8*, 1680.

TOC

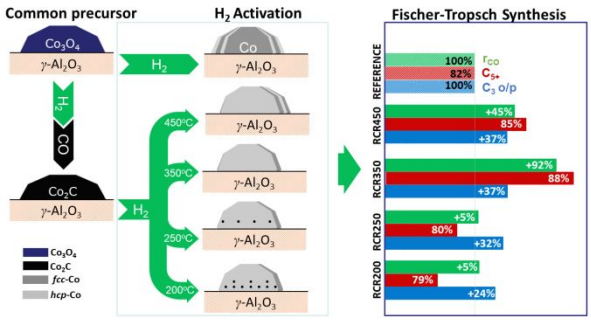
Common precursor
H2 Activation
Fischer-Tropsch Synthesis
Co3O4
γ-Al2O3
H2
Co
CO
Co2C
450°C
350°C
250°C
200°C
Co3O4
Co2C
fcc-Co
hcp-Co
REFERENCE
RCR450
RCR350
RCR250
RCR200
100%
82%
100%
rCO
C5+
C3 o/p
+45%
85%
+37%
+92%
88%
+37%
+5%
80%
+32%
+5%
79%
+24%

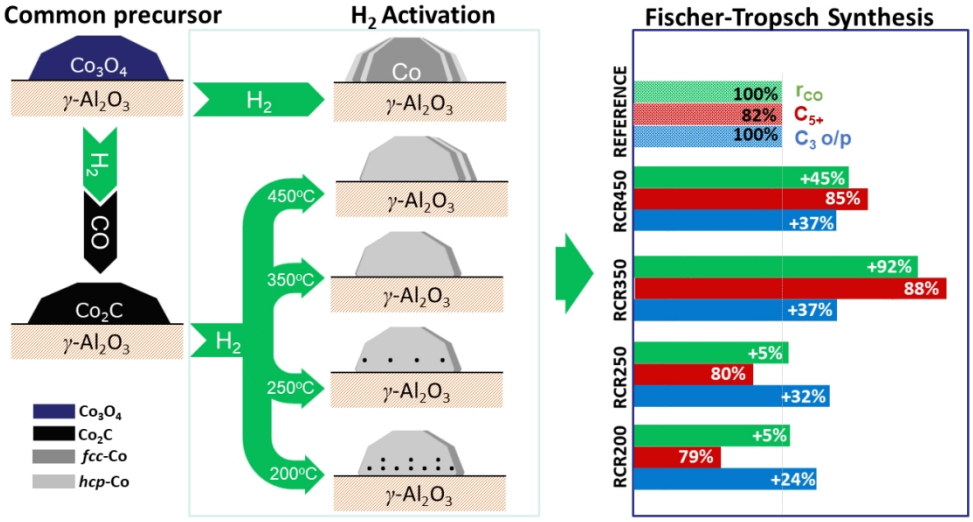

Table of Contents Graphic

360x189mm (96 x 96 DPI)